# Characterization of Mutant Xylanases Using Fourier Transform Ion Cyclotron Resonance Mass Spectrometry: Stabilizing Contributions of Disulfide Bridges and N-Terminal Extensions†

Janne Jänis,‡ Ossi Turunen,§ Matti Leisola,§ Peter J. Derrick,|| Juha Rouvinen,‡ and Pirjo Vainiotalo*,‡

*Department of Chemistry, University of Joensuu, P.O. Box 111, FI-80101 Joensuu, Finland, Laboratory of Bioprocess Engineering, Helsinki University of Technology, P.O. Box 6100, FI-02015 HUT, Finland, and Department of Chemistry, Institute of Mass Spectrometry, University of Warwick, Coventry CV4 7AL, United Kingdom*

*Received February 27, 2004; Revised Manuscript Received May 17, 2004*

ABSTRACT: Structural properties and thermal stability of *Trichoderma reesei* endo-1,4-$\beta$-xylanase II (TRX II) and its three recombinant mutants were characterized using electrospray ionization Fourier transform ion cyclotron resonance (ESI FT-ICR) mass spectrometry and hydrogen/deuterium (H/D) exchange reactions. TRX II has been previously stabilized by a disulfide bridge C110−C154 and other site-directed mutations (TRX II mutants DS2 and DS5). Very recently, a highly thermostable mutant was introduced by combining mutations of DS5 with an N-terminal disulfide bridge C2−C28 (mutant DB1). Accurate mass measurements of TRX II, DS2, DS5, and DB1 verified the expected DNA-encoded protein sequences (average mass error 1.3 ppm) and allowed unequivocal assignment of the disulfides without chemical reduction and subsequent alkylation of the expected cross-links. Moreover, H/D exchange reactions provided means for the detection of a major heat-induced conformational change comprising two interconverting conformers of very different H/D exchange rates as well as allowed the apparent melting temperatures ($T_m$) to be determined (62.6, 65.1, 68.0, and 82.2 °C for TRX II, DS2, DS5, and DB1, respectively). Residual activity measurements verified that the enzymes inactivated at significantly lower temperatures than expected on the basis of the apparent $T_m$ values, strongly suggesting that the inactivation takes place through minor conformational change other than observed by H/D exchange. ESI FT-ICR analyses also revealed molecular heterogeneity in DS5 and DB1 due to the propeptide incorporation. Resulting unintentional N-terminal extensions were observed to further improve the stability of the DB1 mutant. The extension of six amino acid residues upstream from the protein N-terminus increased stability by ∼5 °C.

Xylanases are glycosyl hydrolases that catalyze the hydrolysis of xylan, the major hemicellulosic component in hardwoods and terrestrial plants (*1*, *2*). Endo-1,4-$\beta$-D-xylanases (EC 3.2.1.8) are usually classified in the glycosyl hydrolase families 10 and 11 (*3*) on the basis of their sequence and catalytic properties. The hydrolysis of internal $\beta$-1,4 glycosidic bonds between the adjacent xylopyranose units proceeds via a configuration-retaining double-displacement mechanism involving acid/base chemistry of the two conserved catalytic glutamate residues (*4*). Xylanases have a variety of applications, such as roles in animal feeding, baking, and pulp bleaching (*1*, *2*, *5*).

In general, it has been suggested that several reasons contribute to protein stabilization, including better hydrogen bonding, additional cross-links, shorter loop regions, and improved electrostatic or aromatic interactions (*6*−*9*). Thermophilic xylanases have been recently subjected to extensive comparison based on crystal structures and amino acid compositions in relation to their thermal stability (*10*). While some common correlations can be postulated, in most cases a combination of multiple contributions is the basis for the enhanced stability. In practice, thermal stability of xylanases has been improved by addition of disulfide bridges (*11*−*15*), engineering polar side chains into a protein surface (*16*), increasing aromatic interactions (*17*), and other amino acid substitutions (*11*−*21*). Also, positive influences of the extensions in the N-terminus have been demonstrated (*21*, *22*). Apart from the intramolecular factors, intermolecular interactions can also play a role in stabilization. For instance, addition of polyols in solution has increased thermal stability of xylanases (*23*−*25*).

*Trichoderma reesei* produces at least four endo-1,4-$\beta$-D-xylanases, of which TRX I[1] and TRX II (formerly named XYNI and XYNII) are the most characterized (*26*, *27*). The three-dimensional structure of TRX II (∼21 kDa, p*I* 9.0) consists of a single domain comprising two $\beta$-sheets and a single three-turn $\alpha$-helix, resembling the shape of a partly closed right hand. TRX II is an industrially relevant enzyme

† This work was financially supported by the Marie Curie Fellowship under the European Union Fifth Framework Program (Grant HPMT-CT-2001-00366), University of Warwick, and the Graduate School of Bioorganic and Medicinal Chemistry in Finland.

* To whom correspondence should be addressed. Tel: +358 13 251 3362. Fax: +358 13 251 3360. E-mail: pirjo.vainiotalo@joensuu.fi.

‡ University of Joensuu.

§ Helsinki University of Technology.

|| University of Warwick.

10.1021/bi049597b CCC: $27.50 
Published on Web 07/02/2004

that has an apparent activity optimum at 55−62 °C and pH 5−6. However, the enzyme is only marginally stable at temperatures beyond 55 °C (half-life ~0.5 min at 65 °C) (*15*). From the perspective of its potential applications, such as pulp bleaching, thermal stability of TRX II should be considerably improved. Introduction of multiple arginines into the "Ser/Thr surface" (*16*), addition of a disulfide C2−C28 in the N-terminal region (*14*), and a combination of the disulfide C110−C154 that anchors the α-helix to the adjacent loop region together with other weakly stabilizing mutations (*15*) have considerably increased the thermal stability of TRX II. Very recently, stability was further improved by a combination of two disulfides, C2−C28 and C110−C154, and three other mutations (Turunen et al., unpublished data).

The advent of electrospray ionization (ESI) has opened up mass spectrometry (MS) as one of the most powerful analytical techniques for structural and functional characterization of proteins (*28*). ESI MS is a very sensitive technique (typically few picomoles consumed during analysis) with the capability of ionizing samples from near-native solution conditions. An intrinsic property in ESI, the formation of multiple charged ions, can be used for characterizing changes in protein structure as the distribution of charge states, albeit not inherently, reflects the solution conformation prior to ionization (*29*). ESI in combination with a Fourier transform ion cyclotron resonance (FT-ICR) mass analyzer (*30*, *31*) represents the most powerful instrumental configuration for protein analyses. FT-ICR yields the highest quality mass spectra in terms of mass accuracy (<1 ppm) and mass resolving power ($R_{fwhm}$ >1000000), providing means for determination of very small molecular differences in proteins, arising from disulfide bridges (*32*), deamidations (*33*), or metal atom oxidation states (*34*).

ESI MS has been successfully used for characterizing heat-induced conformational changes for many different proteins by analyzing changes in charge state distributions (*35*−*37*). Beyond this traditional approach, hydrogen/deuterium (H/D) exchange as a mass spectrometric application has extended possibilities of MS in probing conformational changes (*38*−*43*) in order to obtain both kinetic and thermodynamic data of the transitions. H/D exchange can localize changes in the structure of a protein that does not induce significant unfolding or dramatic change in the surface charging as well as changes in overall stability through large conformational transitions.

We have previously used a combination of ESI FT-ICR mass spectrometry, H/D exchange reactions, and dynamic light scattering (DLS) to successfully characterize the thermal stability of TRX II in various solution conditions (*44*). The results gave interesting insights into heat-induced transitions in TRX II and provided useful data to disentangle reasons for its low intrinsic thermal stability. In this work, we further used the same techniques in order to characterize the structure and stability of genetically engineered TRX II variants with a variety of site-directed mutations, including disulfide bridges and unintended extensions of amino acids upstream of the N-terminus.

```
      -10      -1         10        20        30
w.t.  AEVESVAVEKRQTIQPGTGYNNGYFYSYWNDGHGGVTYTNGPGGQFSVNNW
DS2
DS5                       D                          E
DB1              C        D                 FC       E
      40       50        60        70        80
w.t.  SNSGNFVGGKGWQPGTKNKVINFSGSYNPNGNSYLSVYGWSRNPLIEYYI
DS2
DS5
DB1
      90       100       110       120       130
w.t.  VENFGTYNPSTGATKLGEVTSDGSVYDIYRTQRVNQPSIIGTATFYQYWS
DS2                     C
DS5                     C
DB1                     C
      140      150       160       170       180
w.t.  VRRNHRSSGSVNTANHFNAWAQQGLTLGTMDYQIVAVEGYFSSGSASITVS
DS2               C
DS5               C       H
DB1               C       H
```

FIGURE 1: Sequence alignment of the wild-type TRX II (SwissProt accession code P36217) and its mutants (DS2, DS5, and DB1). Amino acid residues exposed to site-directed mutations are underlined. Only the changed residues are presented for the mutants. Eleven amino acid residues of the N-terminal *T. reesei* xln2 cDNA encoded prosequence (negative numbering) are double underlined. Y27F is an unintentional mutation. The residues susceptible for N-glycosylation are in boldface letters.

## EXPERIMENTAL PROCEDURES

*Protein Production.* Native DNA-encoded TRX II (SwissProt accession code P36217) was produced in a *T. reesei* Rut-C30 strain and purified as previously described in detail (*26*, *27*). The recombinant xylanase mutants were produced in *Escherichia coli*. The details of the generation, expression, and purification of the mutants have been reported elsewhere (*15*; Turunen et al., unpublished data).

*The Mutants.* The TRX II mutant enzymes used in this study were as follows: (1) the mutant DS2 [earlier code was S (*15*)] containing mutations S110C and N154C; (2) the mutant DS5 [earlier SHDE (*15*)] containing mutations N11D, N38E, S110C, N154C, and Q162H; (3) the mutant DB1 that is based on DS5 and contains additional N-terminal cysteines T2C and T28C and an unintended mutation Y27F. Sequence alignment of TRX II and its mutants is presented in Figure 1.

*Sample Preparations*. All chemicals were purchased from Sigma-Aldrich (Sigma-Aldrich Co. Ltd., Gillingham, U.K.) except deuterium oxide (99.9 atom % D), which was purchased from Euriso-top (Euriso-top, Gif-Sur-Yvette, France). The purity of the mutant xylanases and stock solution concentrations were first estimated by SDS−PAGE. Main bands appeared around 20−25 kDa with reasonable purity, but concentrations appeared to be low. Since the samples were originally prepared in sodium citrate/phosphate buffer, further purification was needed prior to mass spectrometric analysis. Stock solutions were first desalted over a PD-10 Sephadex G-25 M column (Amersham Biosciences Ltd., Bucks, U.K.), previously equilibrated with ammonium acetate (10 mM, pH 6.8). Protein-containing fractions were combined and concentrated by Millipore Ultrafree (5 kDa cutoff) centrifugal filter devices (Millipore, MA). Devices were loaded with desalted protein solution and ultrafiltered at 10000 rpm (10621*g*) and 4 °C for 10−15 min using an

[1] Abbreviations: ESI, electrospray ionization; FT-ICR, Fourier transform ion cyclotron resonance; TRX II, *Trichoderma reesei* xylanase II; DS2, single-disulfide mutant of TRX II; DS5, a 5-fold, single-disulfide mutant of TRX II; DB1, a 7-fold, double-disulfide mutant of TRX II; H/D, hydrogen/deuterium; $V_{p-p}$, peak-to-peak voltage; RF, radio frequency; $R_{fwhm}$, mass resolving power defined as $m/\Delta m_{fwhm}$ ($\Delta m_{fwhm}$ = peak full width at half-maximum); PCA, N-terminal pyrrolidonecarboxylic acid; $T_m$, apparent melting temperature; $T_{50}$, temperature with 50% residual activity; MS, mass spectrometry; DSC, dynamic scanning calorimetry; CD, circular dichroism spectroscopy.

Eppendorf 5804R ultracentrifuge (Eppendorf AG, Hamburg, Germany). Protein concentrations were determined by absorbance at 280 nm ($A_{280}$) using a Jasco V-550 spectrophotometer (Jasco Ltd., Great Dunmow, U.K.). For the wild-type TRX II, $A_{280} = 1$ corresponds to a concentration of 0.37 mg $mL^{-1}$ (*15*) leading to a molar extinction coefficient of 54050 $M^{-1}$ $cm^{-1}$, which was used for all protein samples.

*Residual Activity Measurements.* The temperature-dependent inactivation profiles of xylanases were determined by incubating the enzyme samples for 10 min at different temperatures, and then the residual activity was determined by measuring the amount of reducing sugars liberated from 1% birchwood xylan by a standard protocol described earlier (*15*).

*H/D Exchange*. H/D exchange reactions in solution were done in a similar fashion as in our previous study (*44*). Reactions were performed in deuterium oxide ($D_2O$, $pD_{corr}$ 5.0) for predefined times using a digitally controlled Grant heating block (Grant Instruments Ltd., Cambridgeshire, U.K.) set at 20−100 °C. Fully deuterated acetic acid (DOAc-$d_4$) was used to adjust the solution pD. Meterlab PHM220 (Radiometer Analytical, Cedex, France) was used to measure all pH and pD values. The isotopic effect correction was calculated from the relation $pD = pH_{measured} + 0.40$ (*45*), and the obtained values are defined here as $pD_{corr}$. H/D exchange reactions were performed in a constant volume of 100 $\mu$L (5 $\mu$L of protein solution + 95 $\mu$L of $D_2O$ → 95 vol % D), and therefore protein concentrations varied from 1.5 to 34 $\mu$M. After the incubation period, the sample tube was immersed on ice to quench the H/D exchange and measured immediately, typically within 1.5 min. H/D exchange reactions are usually quenched by lowering the solution pH to ~2.5 at 0 °C, which effectively slows down the amide proton H/D exchange (*39*). However, to observe changes in the protein charge state distributions upon heat-induced transitions, the pH was not lowered in our case.

*Mass Spectrometry.* Mass spectrometric measurements were performed using two Bruker BioAPEX ESI FT-ICR instruments (Bruker Daltonics, Billerica, MA), referred to here as 9.4 and 4.7 T. The first instrument consists of an external ESI source (Analytica of Branford, Branford, CT), a 9.4 T central-field passively shielded superconducting magnet (Magnex Scientific Ltd., Abingdon, U.K.), and an Infinity ICR cell (*46*). This instrument was described earlier in detail (*47*). Carbon dioxide ($CO_2$), at 250 °C and 20 psi, was used as a countercurrent drying gas. The sample was delivered to the ion source by a Cole-Parmer 74900 series syringe infusion pump (Cole-Parmer Instrument Co., Vernon Hills, IL) at a flow rate of 1.5 $\mu$L $min^{-1}$ using Hamilton gastight 1700 RN syringes (Hamilton Bonaduz, AG, Switzerland). Capillary entrance, cylinder, and end-plate electrode potentials were set to −5.3, −3.5, and −4.9 kV, respectively. The glass capillary exit potential was maintained at 120 V. ESI-generated ions were accumulated for 4 s in a radio frequency (RF) hexapole ion trap (operated at 5.2 MHz and 500 $V_{p-p}$), before being extracted from the source (extraction pulse P2 = 5.5 ms) and transferred to the ICR cell for trapping, excitation, and detection.

The second instrument is based on a 4.7 T passively shielded superconducting magnet (Magnex Scientific), an Apollo ESI source (Bruker Daltonics), and an Infinity ICR cell. This instrument is partly described elsewhere (*44*). Apollo ESI source construction and performance are briefly described here. Sample solution was passed through a 10 cm stainless steel capillary at a flow rate of 1.5 $\mu$L $min^{-1}$ (held at earth potential) as with 9.4 T to generate the electrospray. $CO_2$ was used as a drying gas (120 °C, 10 psi) as well as a nebulizing gas (15 psi). Ions were collected at an end-plate electrode (−4.5 kV) and passed through a dielectric glass capillary (entrance and exit potentials −4.9 kV and 180 V, respectively). Ions then entered through the first skimmer (5 V) to a 1 cm RF hexapole (5.2 MHz and 550 $V_{p-p}$) that focused ions through the second skimmer (15 V) before they entered into a 6 cm RF hexapole (5.2 MHz, 550 $V_{p-p}$, DC offset 0.78 V), in which they were accumulated for 500 ms. After the accumulation period ions were extracted from the source (P2 = 5.0 ms) and transferred to the ICR cell.

At both the 9.4 and 4.7 T instruments, ions were trapped by a SideKick technique prior to frequency sweep excitation (36−96 kHz, 15 $\mu$s, 72 $V_{p-p}$) and broad-band detection. Cell parameters were adjusted to obtain high resolution and high mass accuracy. Trapping plates (PV1 and PV2) were typically set to 1.0 V and SideKick electrodes (EV1, EV2, and DEV2) to appropriate values. The measurements were carried out with 512K (524288) data points and consisted of 128 (9.4 T) or 8 (4.7 T) coadded time-domain transients. The recorded transients were subjected to fast Fourier transform, magnitude calculation and finally zero-filled once. Mass spectra were externally calibrated using the most abundant isotopic peaks from the horse heart myoglobin (Swiss-Prot accession code P02188) or the commercial calibrant mixture (ES Tuning Mix; Hewlett-Packard, Palo Alto, CA). Mass spectral acquisition and postprocessing were performed on Bruker XMASS 5.1 software. Protein elemental composition and theoretical isotope distribution analyses were done using a ProtParam tool (available at ExPaSy Proteomics Server; http://expasy.org/) and XMASS 6.0.

## RESULTS

*9.4 T ESI FT-ICR Analyses*. Figure 2 presents 9.4 T ESI FT-ICR mass spectra of the wild-type TRX II and its mutants measured in 10 mM ammonium acetate (pH 6.8) buffer. All spectra exhibited distribution of charge states ranging from 7+ to 10+. Using either water or methanol/water solutions within pH 3.0−7.0 (data not presented) resulted in negligible changes in the overall spectral appearance from that obtained in ammonium acetate buffer at pH 6.8. However, using acetonitrile/water/acetic acid (49.5:49.5:1.0 v/v, pH 3.0) solution instead changed the appearance of charge state distribution considerably toward the higher charge states (Figure 3). As the distribution of observed charges with an FT-ICR instrument having the external ion source is highly influenced by the "time-of-flight effect" (*48*), a consequence of the extraction pulse (P2) duration that limits the *m*/*z* range to be detected, P2 was varied between 3.0 and 5.5 ms in order to see the apparent effects on the charge state distributions of TRX II. In ammonium acetate buffer, however, no changes were observed within the charge state distribution with P2 values 3.0−5.5, except the absolute ion intensity variation (data not shown), suggesting a single conformation present in solution. In contrast, clear changes appeared in the presence of acetonitrile. Panel A in Figure 3 presents the TRX II mass spectrum recorded with a P2 of

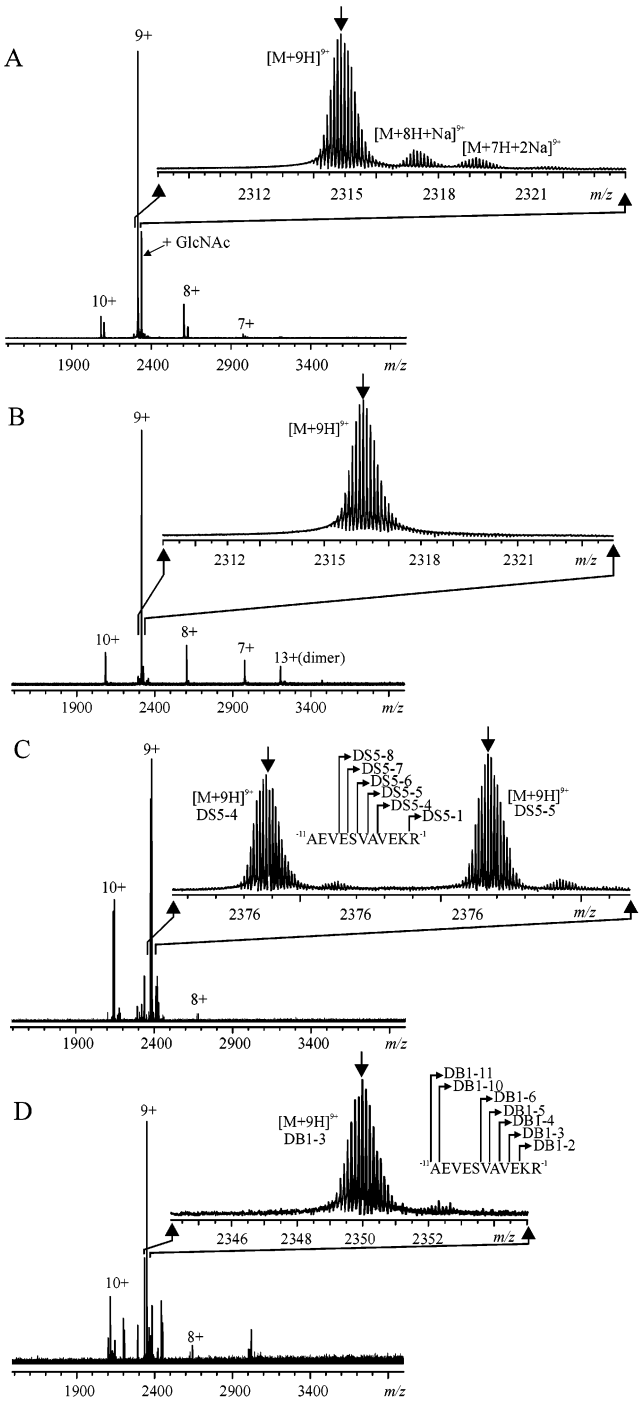


FIGURE 2: 9.4 T ESI FT-ICR mass spectra of (A) 5.3 $\mu$M TRX II, (B) 8.5 $\mu$M DS2, (C) 10.3 $\mu$M DS5, and (D) 7.3 $\mu$M DB1 in 10 mM ammonium acetate (pH 6.8). Numbers ($n$+) denote charge states as $[M + nH]^{n+}$. The expansions show isotopically resolved 9+ charge states ($R_{fwhm}$ exceeds 140000). The arrows indicate the isotopic peaks corresponding to the most abundant isotopic masses as listed in Table 1. Heterogeneous N-terminal prosequence incorporations in DS5 and DB1 are schematically presented in the expansions of the corresponding mass spectra (panels C and D).

5.5 ms, whereas panel B presents the spectrum with P2 decreased to 4.5 ms. In panel B, a bimodal charge state distribution centered around charge states 10+ and 15+ is clearly observed, suggesting that in these solution conditions TRX II exists in, at least, two different conformations, one representing a denatured, "random-coil" protein form (average charge 15+) whereas the other representing a more

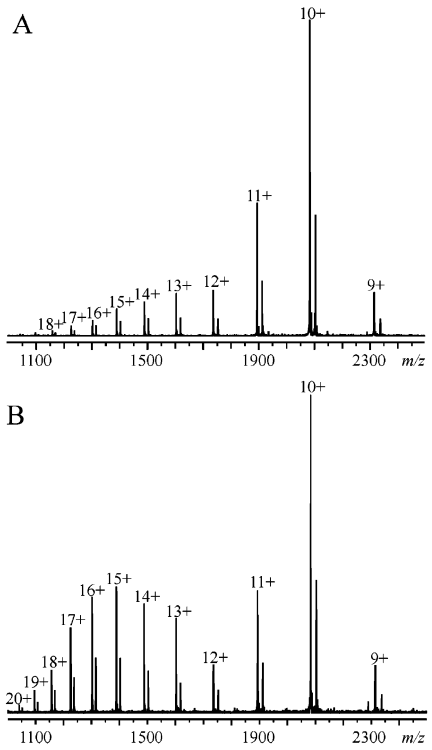


FIGURE 3: 9.4 T ESI FT-ICR mass spectra of 5.3 $\mu$M TRX II measured in acetonitrile/water/acetic acid (49.5:49.5:1.0 v/v) solution: (A) ion source extraction pulse duration (P2) set to 5.0 ms and (B) P2 decreased to 4.5 ms. Numbers ($n$+) denote charge states as $[M + nH]^{n+}$.

folded conformer (10+). These findings are congruent with our previous findings with TRX II (*44*). The observations therefore highly promote the argument that the charge state distributions of TRX II and three mutants obtained in either 10 mM ammonium acetate or water solutions at pH 3.0−7.0 (centered around the 9+ charge state) reflect their native, folded conformations. This argument is supported by the finding that TRX II has 8−10 basic amino acid residues on its surface (*44*). Moreover, TRX II retains full activity in the pH ranges 3.0−8.5 at room temperature and 4.0−7.5 at 40 °C at least for 24 h (*49*). To ensure near-native conditions, temperature-dependent H/D exchange reactions were therefore performed at $pD_{corr}$ 5.0.

Native TRX II had two adjacent peaks in each charge state separated by a mass increment of 203 Da, consistent with N-glycosylation by a single *N*-acetyl-D-glucosamine residue (see Figures 2 and 3), but the mutants expressed from *E. coli* did not have peaks corresponding to that modification. The site and the identity of the modification were not further studied.

Unexpectedly, DS5 and DB1 mutants had a substantial molecular heterogeneity in the samples resulting in a distribution of peaks in each charge state (Figure 2, panels C and D). Detailed analysis showed that these peaks correspond to a heterogeneously incorporated N-terminal *T. reesei* prosequence of 11 residues (AEVESVAVEKR) that is present in the *E. coli* pALK143 expression vector construct (*15*, *50*). It has been assumed that the prosequence is cleaved out during expression by an extracellular protease, which has now been found not to be the case. Different protein forms of DS5 (six forms) and DB1 (seven forms) are assigned in the expansions of the ESI FT-ICR spectra (Figure

Table 1: Modifications, Accurate Masses, and Standard Deviations for Disulfide Bridge Assignment of TRX II and Its Recombinant Mutants Based on 9.4 T ESI FT-ICR Measurements

| protein code[a] | modification | $M_{exp}$ (Da)[b] | $M_{theor}$ (Da)[c] | $\Delta M$ (ppm) | standard deviation[d] $\sigma_{ox}$ | $\sigma_{red}$ | $\sigma_{2red}$ | disulfide bridges[e] |
|---|---|---|---|---|---|---|---|---|
| wt | PCA(Q1) | 20824.839 ± 0.035 | 20824.850 | −0.5 | | | | 0 |
| DS2 | PCA(Q1) | 20827.835 ± 0.030 | 20827.782 | +2.6 | 0.03 | 0.26 | | 1 |
| DS5-4 | prosequence[f] | 21454.158 ± 0.011 | 21454.122 | +1.7 | 0.07 | 0.29 | | 1 |
| DS5-5 | prosequence | 21382.112 ± 0.018 | 21382.082 | +1.4 | 0.10 | 0.32 | | 1 |
| DB1-2 | prosequence | 21012.811 ± 0.016 | 21012.790 | +1.0 | 0.05 | 0.27 | 0.46 | 2 |
| DB1-3 | prosequence | 21140.902 ± 0.026 | 21140.885 | +0.8 | 0.04 | 0.28 | 0.47 | 2 |
| DB1-11 | prosequence | 22054.306 ± 0.010 | 22054.325 | −0.9 | nc[g] | nc | nc | 2[h] |

[a] For mutations, see text and Figure 1. Code suffixes in DS5 and DB1 refer to the number of incorporated prosequence residues upstream of the N-terminus; see Figure 2. [b] The average experimental value of the most abundant isotopic mass over the charge state distribution ± standard deviation. [c] The most abundant isotopic mass calculated from the sequence-based elemental composition (all cysteines are presumed to be oxidized). [d] The standard deviations between experimental and calculated isotopic distributions from the most abundant charge states (for details, see text and Figure 4): $\sigma_{ox}$, all cysteines oxidized; $\sigma_{red}$, one disulfide reduced; and $\sigma_{2red}$, two disulfides reduced (the smallest deviation underlined). [e] Number of observed disulfide bridges based on standard deviation calculations (for details, see text and Figure 4). [f] N-Terminal prosequence incorporation (see Figure 2). [g] nc = not calculated. [h] Based on the mass difference.

2, panels C and D) using a code suffix *X* (DS5-*X*, DB1-*X*) that corresponds to the prosequence numbering (Figure 1).

The results from the accurate mass measurements of TRX II and its mutants are summarized in Table 1. The isotopic peaks corresponding to the most abundant isotopic masses listed in Table 1 are denoted by arrows in the expansions of the ESI FT-ICR spectra in Figure 2. The masses verified that both TRX II and the DS2 mutant had an N-terminal glutamine residue in its cyclic pyrrolidonecarboxylic acid form (PCA; −17.027 Da). Due to the prosequence incorporation in the N-terminus, DS5 and DB1 did not have that modification. The unintentional mutation Y27F in DB1 (appeared in the cDNA sequencing) was also unambiguously resolved by the 9.4 T ESI FT-ICR analyses.

*Verification of Disulfides.* Interpretation of the 9.4 T ESI FT-ICR mass data suggested that DS2 and DS5 had one and DB1 had two disulfide bridges (Table 1). However, the assignment of the most abundant isotopic mass at every charge state was not straightforward due to the deviations in vertical precision of adjacent isotopic peaks. Theoretically, the abundance ratio of the most and the second most abundant isotopic composition in DS2 is ∼0.995, which exacerbates the visual assignment of the corresponding peaks, particularly in view of detector noise. Hence, to verify the number of disulfide bridges (i.e., to take into account a possible misinterpretation of the mass spectral peaks), an approach based on a standard deviation ($\sigma$) calculation between experimental and theoretical isotopic distributions (*34*) was used:

$$\sigma = \sqrt{\sum (I_{exp} - I_{theor})^2/(N-1)}$$

in which $I_{exp}$ and $I_{theor}$ are the experimental and theoretical relative abundance of the peaks representing each isotopic mass (the highest in a given distribution is scaled to unity) and $N$ is the number of resolved above-threshold isotopic peaks. This approach requires high resolving power and undistorted ion isotopic distributions for all peaks that will be incorporated and compared. Comparison of the experimental and theoretical isotopic distributions of the $[M + 9H]^{9+}$ ion of DS2 is presented in Figure 4. Standard deviations between experimental and theoretical isotopic distributions, defined as $\sigma_{ox}$ (all cysteines oxidized), $\sigma_{red}$ (one disulfide reduced), and $\sigma_{2red}$ (two disulfides reduced; in DB1 only) were used to assign the correct number of disulfide bridges, i.e., which gives the smallest deviation. Results of standard deviation calculations (Table 1) are in agreement with suggested numbers of disulfide bridges based on accurate masses of all mutants, by all giving the smallest value for $\sigma_{ox}$.

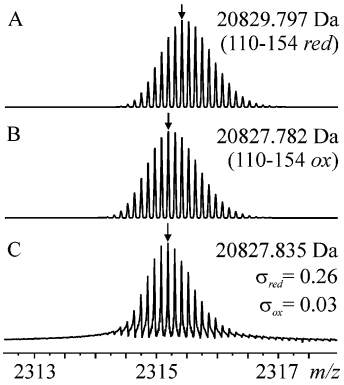


FIGURE 4: Theoretical and experimental ion isotopic distributions of the $[DS2 + 9H]^{9+}$ ion. Panels A and B show isotopic distributions with disulfide C110−C154 oxidized (A) or reduced (B), whereas panel C represents the experimental distribution obtained from the 9.4 T ESI FT-ICR mass spectrum in Figure 2, panel B. Arrows indicate the isotopic peaks corresponding to the most abundant isotopic masses listed in the upper right corners of the panels. In panel C, calculated standard deviations between the experimental and two calculated isotopic distributions have been presented (see text for details). Theoretical isotopic distributions were calculated using XMASS 6.0 from sequence-derived elemental composition of DS2.

*Thermal Stability*. The thermal stability of TRX II and its mutants was studied by H/D exchange as a function of incubation temperature. To optimize the incubation time with respect to H/D exchange kinetics in employed solution conditions, an exchange progress curve for TRX II was generated by plotting the number of exchanged hydrogens as a function of incubation time at 20 °C (Figure 5). Data in Figure 5 address that incubation times greater than 6 min resulted in ∼100% exchange level (∼160 hydrogens) for all exchangeable hydrogens in employed conditions. The pseudo-first-order exchange rate constants (*39*) were obtained by fitting the experimental data points, using the nonlinear least-squares routine in Microcal Origin 5.0 software, to the

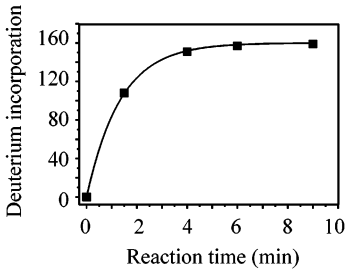


FIGURE 5: Deuterium incorporation in H/D exchange reactions of TRX II by $D_2O$ ($pD_{corr}$ 5.0) at 20 °C as a function of the reaction time. An average number of incorporated deuteriums were calculated from the centroid masses of the isotopic distributions as stated in Experimental Procedures. The solid curve is the best double-exponential fit to the experimental data points.

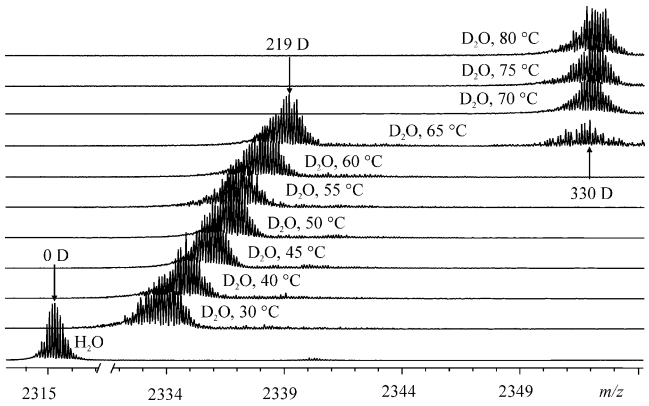


FIGURE 6: Expansions on the isotopically resolved 9+ charge state of 4.7 T ESI FT-ICR mass spectra of DS2 (6.3 $\mu$M) in $H_2O$ + 0.025% (v/v) acetic acid and after 10 min incubation in $D_2O$ ($pD_{corr}$ 5.0) at 30−80 °C. An average number of incorporated deuteriums after the incubation at 65 °C for the folded and open conformers are presented (the corresponding isotopic peaks are denoted by arrows).

expression of two exponential terms:

$$D(t) = H_{total} - a(H_{fast}e^{-k_{fast}t} + H_{slow}e^{k_{slow}t})$$

in which $H_{total}$ is a total number of exchangeable hydrogens in TRX II (341 based on the sequence), $a$ is a D/H ratio in solution (0.95), $H_{fast}$ and $H_{slow}$ are the numbers for fast and slow exchanging hydrogens, and $k_{fast}$ and $k_{slow}$ are the corresponding pseudo-first-order rate constants. The fitting yielded values of $k_{fast} = 0.768 \pm 0.0017$ min$^{-1}$ ($H_{fast} \approx 166$) and $k_{slow} = 0.00097 \pm 0.00014$ min$^{-1}$ ($H_{slow} \approx 193$), indicating that ~166 hydrogens were fast exchanged upon the local structural fluctuations. In constrast, ~193 hydrogens were buried into the protein interior, and these hydrogens become exchanged only upon very infrequent global unfolding events as the interior is exposed to solvent. As $k_{fast}$ was almost three magnitudes higher than $k_{slow}$, 10 min was chosen as an appropriate time for H/D exchange reactions in order to avoid any errors from kinetic reasons, e.g., slight variations in the time gap between reaction quench and mass measurement or the forward exchange occurring during the sample delivery to the ion source.

Figure 6 shows isotopically resolved 4.7 T ESI FT-ICR mass spectra, expanded in the 9+ charge state of the DS2 mutant after the incubation for 10 min at 30−80 °C in $D_2O$ ($pD_{corr}$ 5.0). Between 20 and 56 °C, deuterium incorporation increases with increasing temperature, implying that the H/D exchange reaction of the folded protein follows an EX2 mechanism (*39*). A clear change appears at 60−70 °C, in which a two-state conformational change takes place as verified by two distinct peaks at each charge state, the one representing a folded whereas the other representing a more open conformer. This behavior is consistent with H/D exchange kinetics following an EX1 mechanism (*39*). The same behavior was evident also for TRX II and other mutants (DS5, DB1). This observation agrees with the previous findings with TRX II (*44*). Deuterium incorporation as a function of incubation temperature for each protein is presented in Figure 7. Average numbers of the exchanged hydrogens ($D$) were calculated using the centroid masses:

$$D = \frac{1}{i}\sum_{n=1}^{i}\frac{\sum_{N}(I_n n - n \times 1.00728)}{\sum_{N} I_n} - M_{exp}$$

in which $I_n$'s are relative abundances of the $N$ isotopic peaks averaged over the $i$ charge states ($n$ is the number of elemental charges in the $i$th charge state), $M_{exp}$ is the most abundant isotopic mass of an unexchanged protein from Table 2, and 1.00728 is the mass of a proton in daltons.

To estimate the apparent melting temperatures ($T_m$)[2] for the proteins, the fractions of the folded conformers ($f_F$) after incubation at each temperature were obtained from the absolute peak heights in ESI FT-ICR spectra using the expression

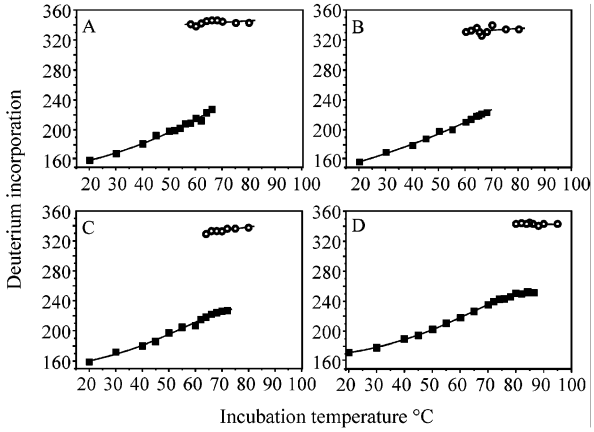


FIGURE 7: Average deuterium incorporation in $D_2O$ ($pD_{corr}$ 5.0) as a function of the incubation temperature for TRX II (A), DS2 (B), DS5-5 (C), and DB1-2 (D). Solid squares denote the folded and open circles the open conformer. Average numbers of exchanged hydrogens were calculated using the centroid masses of the observed isotopic distributions over $i$ charge states. Experimental data points are average values from three replicate measurements.

[2] Thermodynamic treatment of the two-state protein denaturation inherently implies a reversible process. Since the conformational change in TRX II is known to be irreversible (*44*), the $T_m$ values are stated as "apparent" values in this context for differentiation from the true thermodynamic values. Change in the reversibility due to mutations was not considered, as H/D exchange reactions performed during heating do not provide such information.

$$f_F = \frac{\sum_{N,i} I_F}{\sum_{N,i} I_F + \sum_{N,i} I_O}$$

in which $I_n$ are the abundance of the peaks representing the folded (F) and open (O) conformers summed over the isotopic distributions ($N$) as well as the charge states ($i$) in H/D exchange ESI FT-ICR mass spectra. Especially for the mutants, this should give a valid response on the relative amounts in solution since the ionization efficiencies between different conformers are likely to be similar as dictated by the unchanged charge state distributions. Then $f_F$ for each protein was plotted versus the incubation temperature (Figure 8), and $T_m$ values were estimated from the transition curves obtained by fitting the experimental data points to the sigmoidal expression $f_F = 1/(1 + e^{(T-T_m)/\Delta T})$ using the nonlinear least-squares routine in Microcal Origin 5.0 software. From these transition curves, the apparent[2] $T_m$ values (i.e., the temperature at which $f_F = 0.5$) were estimated to be 62.6, 65.1, 68.0, and 82.2 °C for TRX II, DS2, DS5-5, and DB1-2, respectively.

In addition, a moderate shift between the charge state distributions of the folded and the open conformers of TRX II was observed (data not shown). The average charge state shifted from 9.4 to 10.3, and the distribution became wider, consistent with our previous results (*44*). Briefly, an average charge state $\langle n \rangle$ can be calculated from the mass spectrum of the multiply charged protein:

$$\langle n \rangle = \frac{\sum_{N,i} nI_n}{\sum_{N,i} I_n}$$

in which $n$ is a nominal charge and $I_n$ is the relative abundance of $N$ above-threshold mass spectral peaks in a given distribution of $i$ charge states (*36*). However, charge state distributions of the folded and open conformers of the mutants were identical within the error level of the experiments. Normalized charge state profiles and calculated average charge states for the folded and open conformers of TRX and its mutants are presented in Figure 9 (the minor protein forms were excluded).

*Influence of N-Terminal Extensions on Stability.* The possibility of the molecular heterogeneity observed in DS5 and DB1 mutants affecting the thermal stability was further examined. Presented charge state profiles, average charge states, numbers of exchanged hydrogens, and unfolding curves were established using the major protein forms of DS5 and DB1, excluding the species with low abundance. Relative abundances of these protein forms varied slightly over the time, indicating that the amino acid residues were slowly cleaved from the N-terminus. As the influence of N-terminal insertions on the stability of xylanases has been previously demonstrated (*21*, *22*), the H/D exchange data were carefully reexamined to distinguish any differences between the species arising from heterogeneous N-terminal prosequence incorporation in DS5 and DB1. On the basis of H/D exchange reactions, the stabilities of the forms of DS5 were identical. However, in the case of DB1, the relative

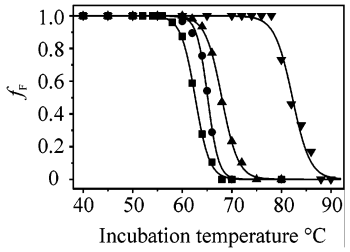


FIGURE 8: Transition curves for heat-induced conformational change: TRX II (squares), DS2 (spheres), DS5 (triangles), and DB1 (reversed triangles). This figure shows the relative abundance of the folded conformer ($f_F$) for each protein after 10 min incubation at 40−90 °C. The apparent melting temperature ($T_m$) is the temperature at which $f_F = 0.5$. Solid curves are the best sigmoidal fits to the experimental data points.

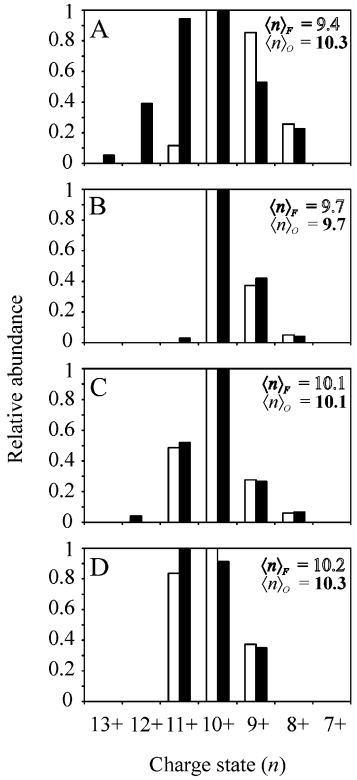


FIGURE 9: Charge state distribution profiles of the folded (white, F) and the open (black, O) conformers of TRX II (A), DS2 (B), DS5-5 (C), and DB1-2 (D). Relative abundances are average values from temperature regions where the corresponding conformer is present. Calculated average charge states of the distributions are presented in the upper right corners of the panels (for calculation details, see text).

abundances of the folded and the open conformers in H/D exchange mass spectra (Figure 10) unambiguously indicated that the longer the extension in the N-terminus, the higher the stability of the corresponding protein form. The apparent $T_m$ value of the form DB1-6 was estimated to be ≥87 °C, which is at least 4.8 °C higher than the $T_m$ value of the major form DB1-2 (82.2 °C). The major form DB1-2 already had two additional residues (KR) from the N-terminal prosequence.

*Residual Activity Measurements.* Besides calorimetric techniques, measurements of inactivation kinetics have been traditionally performed to study thermally induced changes in proteins. Previously, the wild-type TRX II, DS2, and DS5 have been exposed to activity assays in order to characterize

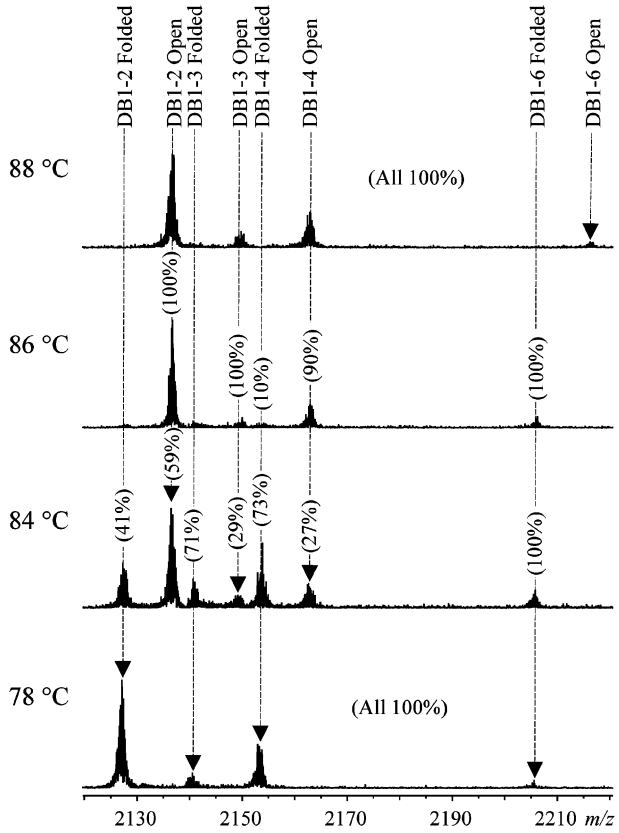


FIGURE 10: Partial 4.7 T ESI FT-ICR mass spectra (9+ charge state) of DB1 after 10 min incubation at 78, 84, 86, and 88 °C in $D_2O$ ($pD_{corr}$ 5.0). Peaks of the different protein forms as well as different conformers are denoted with the numbers that refer to the sequence alignment in Figure 1. Relative abundances (calculated over all charge states) for the folded and open conformers of the corresponding form are in parentheses.

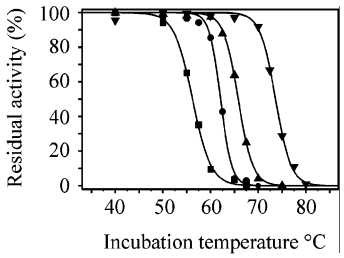


FIGURE 11: Temperature-dependent inactivation profiles of TRX II (squares), DS2 (spheres), DS5 (triangles), and DB1 (reversed triangles). Enzyme samples were incubated for 10 min at each temperature prior to residual activity measurements. Residual activity of 100% corresponds to the value of TRX II at 40 °C (for details, see text). Solid curves are the best sigmoidal fits to the experimental data points.

stability profiles at high temperatures (*15*). Comparison with the presented mass spectrometric results, however, was not reliable as different solution conditions were employed. Residual activity measurements were therefore performed at the same conditions that were utilized in H/D exchange reactions. Figure 11 represents residual activity of the wild-type TRX II and the mutants after 10 min heatings at 40−80 °C and pH 5.0. Inactivation curves demonstrate that the $T_{50}$ values (i.e., the temperature at which 50% of the original activity remains after 10 min incubation) were clearly lower than the corresponding $T_m$ values for all of the enzymes. Table 2 summarizes the observed $T_m$, $T_{50}$, and the calculated

Table 2: Apparent $T_m$ and $T_{50}$ Values for TRX II and Its Recombinant Mutants (Major Forms)

| protein code[a] | $T_m$ (°C)[b] | $\Delta T_m$ (°C) | $T_{50}$ (°C)[c] | $\Delta T_{50}$ (°C) | $\Delta(T_m - T_{50})$ (°C) |
|---|---|---|---|---|---|
| wt | 62.6 ± 0.1 | | 56.2 ± 0.4 | | +6.4 |
| DS2 | 65.1 ± 0.1 | +2.5 | 62.1 ± 0.2 | +5.9 | +3.0 |
| DS5-5 | 68.0 ± 0.1 | +5.4 | 65.8 ± 0.2 | +9.6 | +2.2 |
| DB1-2 | 82.2 ± 0.2 | +19.6 | 73.6 ± 0.4 | +17.4 | +8.6 |

[a] For code assignment, see Figure 2. [b] $T_m$ is the apparent melting temperature based on H/D exchange and mass spectrometry (the reported error is twice the standard error obtained by the fitting procedure). [c] $T_{50}$ is the temperature at which the residual activity of 50% remains after 10 min incubation (the reported error is twice the standard error obtained by the fitting procedure).

$\Delta(T_m - T_{50})$ values. The apparent $T_m$ value for DB1-2 was even 8.6 °C higher than the corresponding $T_{50}$ value.

## DISCUSSION

A high-resolution mass spectrometry was successfully used in probing the contributions of disulfide bridges and other site-directed mutations on the thermal stability of TRX II. The accurate mass data confirmed that all amino acid substitutions were successfully engineered by site-directed mutagenesis. Molecular heterogeneity that was present in DS5 and DB1 mutants due to the partial prosequence incorporation did not complicate the analysis, since the high resolving power ($R_{fwhm}$ typically exceeding 140000) and high mass accuracy (the average error within the most abundant isotopic masses $|\Delta M|_{average} = 1.3$ ppm) of the ESI FT-ICR MS provided means for unequivocal assignment of different protein forms. The isotopically resolved mass spectrum readily provides a number of elemental charges ($z$) for a species observed at a given $m/z$, since the reciprocal of the spacing between the adjacent isotopic peaks, $(m_{i+1} - m_i)^{-1}$, equals $z$. When $z$ and $m/z$ are accurately known, $m_i$ can be unambiguously calculated.

The accurate masses of DS2, DS5, and DB1 suggested that disulfides C2−C28 and C110−C154 had been formed (Table 1). Standard deviation calculations between the theoretical and the experimental isotopic distributions confirmed the expected number of disulfides in DS2, DS5, and DB1 mutants (i.e., one in both DS2 and DS5 and two in DB1). Selective reduction protocols and FT-ICR mass spectrometry can provide means for detecting disulfide bridges in proteins. Such approach has been used to differentiate between reduced and unreduced forms of proteins having numerous disulfide bridges (*37*). Reduction of each disulfide gives rise to a mass increment of +2.016 Da. Our results indicate that high-field FT-ICR mass spectrometry could be used to unequivocally assign the number of disulfide bridges without chemical reduction and alkylation of disulfides if elemental compositions (i.e., protein sequences) are accurately known.

The wild-type TRX II produced in *T. reesei* had two adjacent peaks in each charge state of the mass spectra due to the N-glycosylation, comprising more than 30% of the total protein content based on the peak heights. This observation was also made in the previous study (*44*). According to the homology consensus N-X-S/T-Z, where Z and X ≠ P, there are only two such putative subsites in TRX

II for N-glycosylation, N38(WSN) and N61(FSG).[3] However, the presence of N appears considerably more favorable than G at the Z-position according to previously published data (*52*). This would tend to favor N38 over N61 as the most likely site for N-glycosylation. Nonetheless, we did not try to experimentally locate and further identify the modification. The N-glycosylation by a single *N*-acetyl-D-glucosamine has been rarely so far observed. However, it has been reported previously for *T. reesei* cellobiohydrolase I (*53*, *54*) and for *Chaetomium thermophilum* xylanase (*10*), but its biological significance is not known.

As previously reported, TRX II expressed from *T. reesei* had approximately three times higher stability than TRX II expressed from *E. coli* based on the inactivation profiles (*15*, *21*). This has been suggested to arise from the posttranslational glycosylation. The results of our present study do not support this conclusion, since the nonglycosylated and the glycosylated protein behaved equally in the stability measurements using H/D exchange mass spectrometry (data not presented). The variation in stability could also arise from the sequence differences in the N-terminus, e.g., extensions from the prosequence, between the enzymes expressed either from *T. reesei* or from *E. coli*. However, we did not have TRX II from *E. coli* to make such comparison by MS. On the other hand, the ESI FT-ICR mass spectrum of the recombinant DS2 (Figure 2, panel B) verified that no other modifications than those generated by the site-directed mutations and PCA(Q1) were present in the protein structure.

H/D exchange and mass spectrometry have been used to investigate the effects of the site-directed amino acid substitutions on the stability of proteins (*55*−*57*). Replacement of Y64 by L, F, V, or A in cytochrome $c_{533}$ from *Desulfovibrio vulgaris* did not induce any changes in the charge state distributions, while H/D exchange reactions revealed a destabilizing effect in the order of decreasing side chain volume (*55*). Recently, a high-throughput method based on H/D exchange and matrix-assisted laser desorption ionization (MALDI), termed SUPREX, was applied in the quantitative determination of thermodynamic stability of protein variants (*56*, *57*). This method allowed precise measurements over a wide range of stabilities from picomoles of material and provided results agreeable with those obtained by circular dicroism (CD) spectroscopy. In our study, H/D exchange in solution yielded direct observation of the significant heat-induced conformational change that, however, had negligible influence on the charge state distributions of the mutants. The observed two-state conformational transition was agreeable with the results of our previous work (*44*).

The EX1-type H/D exchange mechanism (i.e., the chemical exchange rate, $k_{ex}$, is much more higher than the unfolding rate, $k_u$), which results in two separate peaks of the interconverting conformers (*39*), allowed us to estimate the apparent melting temperatures ($T_m$) from the relative peak abundance in the mass spectra (Figure 9, Table 2). This estimation is conceivable if relative peak heights are assumed to reflect true concentrations in solution, which is valid only in the case of similar ionization efficiencies. As the charge state distributions, particularly for the mutants, were almost insensitive to conformational change, therefore the former assumption could be deduced.

Interestingly, the $T_m$ value for the wild-type TRX II (62.5 °C) was substantially higher than expected based on its inactivation profile (∼53 °C) (*15*) or the earlier value obtained by mass spectrometry (∼55 °C) (*44*). Irreversible transitions in proteins, often triggered by local unfolding (*58*), prevent the true thermodynamic $T_m$ and $\Delta G°$ values to be determined, and therefore the incubation time should be equal while comparing results from the two methods. In our previous work (*44*), a different pH (3.4, uncorrected for isotopic effect) and incubation time (20 min) were employed in H/D exchange reactions for TRX II, and the reported activation profiles (*15*) were measured at pH 8.0. Therefore, in this work the residual activity measurements were performed at pH 5.0 for 10 min in order to make a good comparison between $T_m$ and $T_{50}$ values. Nevertheless, $T_m$ values were significantly higher than the corresponding $T_{50}$ values at pH 5.0 (Table 2). The possible explanation for the difference between these two values could be that the inactivation takes place at lower temperatures (i.e., $T_{50}$) than what is required for the major conformational change ($T_m$). For DB1, this difference was remarkably high (8.6 °C). $\Delta(T_m - T_{50})$ values for all proteins are listed in Table 2. While residual activity is often used as a measure of stability, they are not implicitly dependent on each other. Thus, the activity can be substantially decreased for several reasons, particularly at high temperatures, while overall stability may still be retained. This can originate, for example, from the different conformations of the catalytic amino acids or small structural changes in close proximity of the active site while protein may still be stable from the thermodynamic point of view. Very recently, differential scanning calorimetry (DSC) was used to measure melting temperatures for TRX II and its Y5 mutant (T2C, T28C, K58R, and +191D) (*14*). The measured $T_m$ of the wild-type enzyme, 61.4 °C, is close to the value provided by mass spectrometry ($\Delta T_m = 1.2$ °C), indicating that while mass spectrometry did not provide direct thermodynamic value,[2] there is a good agreement with the calorimetric value obtained by DSC. On the other hand, the $T_m$ values obtained by DSC can also vary as a consequence of the scan rate dependence (*12*).

Charge state distribution is known to be sensitive to protein conformation in solution (*29*). However, only the wild-type TRX II exhibited a change between the two conformers (Figure 9), suggesting the increased stability of DS2, DS5, and DB1 by the disulfide C110−C154. The disulfide bridge mutant of *Bacillus circulans* xylanase (BCX) has been exposed to stability analyses using DSC (*12*). On the basis of the DSC profiles, the disulfide C100−C148, connecting the α-helix to the adjacent loop, enhanced thermal stability of BCX by increasing the rate of refolding and, to a lesser extent, the unfolding rate of the irreversible transition in the urea-free conditions. In general, cross-links, e.g., disulfide bonds, are known to enhance conformational stability by decreasing the entropy of the unfolded state, which originates from the constraints on the protein flexibility (*6*−*8*). Such findings are congruent with the presented results, indicating that the open conformers of the mutants having the disulfide C110−C154 are less flexible than the open conformer of the wild-type TRX II, which results in the increased stability of the folded conformers via entropic effects. In contrast,

[3] N97(PST) was incorrectly interpreted as the third potential N-glycosylation site in our previous report (*44*).

the N-terminal disulfide C2−C28 in DB1 did not alter the charge state distribution profiles but further enhanced stability from that obtained for DS2 or DS5.

While a relatively large heat-induced conformational change took place, the more open protein conformers still exhibited charge state distributions (Figure 9) that do not resemble those observed in the presence of acetonitrile (Figure 3), which obviously induces, at least to some extent, the complete unfolding of the protein having "a random-coil" conformation. Consequently, it is suggested that some degree of secondary structure elements (i.e., $\beta$-sheets) must be preserved during the conformational transition, which precludes the formation of highly charged species due to unfavorable charge−charge repulsions but, however, does not prevent nearly complete deuteration of the molecules. For instance, far-UV CD analysis of the thermally denatured *E. coli* thioredoxin indicated that the protein exhibited a relatively high content of its original tertiary structure at 80 °C, while a considerable heat-induced denaturation was observed using near-UV CD and H/D exchange mass spectrometry (*42*). This type of discrepancy has also been reported for other thermally denatured proteins (*42*). Unfortunately, we did not have access to CD instruments for experimental confirmation of the secondary structure elements in the heat-denatured TRX II conformer.

On the basis of several experimental studies, the three major regions affecting the stability in thermophilic xylanases are the N-terminus, the α-helix, and the Ser/Thr surface (*10*). Our results indicate that the disulfide C2−C28 in TRX II had much higher influence on the stability than the disulfide C110−C154 or other mutations. However, the presence of the N-terminal extensions in DB1 having the N-terminal disulfide C2−C28 seemed to further stabilize the protein based on the H/D exchange data. Therefore, it is evident that the N-terminal region has a considerable importance in thermal stabilization of family 11 xylanases. This argument is supported by the several studies (*11*, *14*, *21*; Turunen et al., unpublished data). However, there is no straightforward explanation for the longer N-terminus to considerably increase the thermal stability. There are other N-terminal extensions reported in the literature that stabilize *T. reesei* xylanase that does not have any disulfide bridges (*21*). A possible explanation for this discrepancy could be that the amino acid sequence of the N-terminal extension in DS5 and DB1 does not have the inherent stabilizing property, without the presence of the disulfide C2−C28. This conclusion is supported by the finding that the same N-terminal extensions did not further stabilize the DS5 mutant.

## ACKNOWLEDGMENT

The authors thank Johanna Aura (Helsinki University of Technology) for technical assistance. We also thank Dr. Mark P. Barrow (University of Warwick) for technical advice during 9.4 T measurements as well as the revision of the manuscript.

## REFERENCES

1. Jeffries, T. (1996) Biochemistry and genetics of microbial xylanases, *Curr. Opin. Biotechnol. 7*, 337−342.
2. Shallom, D., and Shoham, Y. (2003) Microbial hemicellulases, *Curr. Opin. Microbiol. 6*, 219−228.
3. Henrissat, B., and Davies, G. (1997) Structural and sequence-based classification of glycoside hydrolases, *Curr. Opin. Struct. Biol. 7*, 637−644.
4. White, A., and Rose, D. (1997) Mechanism of catalysis by retaining $\beta$-glycosyl hydrolases, *Curr. Opin. Struct. Biol. 7*, 645−651.
5. Viikari, L., Kantelinen, A., Sundquist, J., and Linko, M. (1994) Xylanases in bleaching: from an idea to the industry, *FEMS Microbiol. Rev. 13*, 335−350.
6. Vogt, G., Woell, G., and Argos, P. (1997) Protein thermal stability, hydrogen bonds, and ion pairs, *J. Mol. Biol. 269*, 631−643.
7. Kumar, S., Chung-Jung, T., and Nussinov, R. (2000) Factors enhancing protein stability, *Protein Eng. 13*, 179−191.
8. Németh, A., Kamondi, S., Szilágyi, A., Magyar, C., Kovári, Z., and Závodszky, P. (2002) Increasing the thermal stability of cellulase C using rules learned from thermophilic proteins: A pilot study, *Biophys. Chem. 132*, 229−241.
9. Vogl, T., Brengelmann, R., Hinz, H.-J., Scharf, M., Lötzbeyer, M., and Engels J. (1995) Mechanism of protein stabilization by disulfide bridges: Calorimetric unfolding studies on disulfide-deficient mutants of the α-amylase inhibitor tendamistat, *J. Mol. Biol. 254*, 481−496.
10. Hakulinen, N., Turunen, O., Jänis, J., Leisola, M., and Rouvinen, J. (2003) Three-dimensional structures of thermophilic $\beta$-1,4-xylanases from *Chaetomium thermophilum* and *Nonomuraea flexuosa*: Comparison of twelve xylanases in relation to their thermal stability, *Eur. J. Biochem. 270*, 1399−1412.
11. Wakarchuk, W., Sung, W., Campbell, R., Cunningham, A., Watson, D., and Yaguchi, M. (1994) Thermostabilization of the *Bacillus circulans* xylanase by the introduction of disulfide bonds, *Protein Eng. 7*, 1379−1386.
12. Davoodi, J., Wakarchuk, W., Surewicz, W., and Carey, P. (1998) Scan-rate dependence in protein calorimetry: The reversible transitions of *Bacillus circulans* xylanase and a disulfide-bridge mutant, *Protein Sci. 7*, 1538−1544.
13. Sung, W., and Tolan, J. (2001) Thermostable xylanases, Patent WO 00/29587.
14. Fenel, F., Leisola, M., Jänis, J., and Turunen, O. (2004) A de novo designed N-terminal disulphide bridge stabilizes the *Trichoderma reesei* endo-1,4-$\beta$-xylanase II, *J. Biotechnol. 108*, 137−143.
15. Turunen, O., Etuaho, K., Fenel, F., Vehmaanpera, J., Wu, X., Rouvinen, J., and Leisola, M. (2001) A combination of weakly stabilizing mutations with a disulfide bridge in the α-helix region of *Trichoderma reesei* endo-1,4-$\beta$-xylanase II increases the thermal stability through synergism, *J. Biotechnol. 88*, 37−46.
16. Turunen, O., Vuorio, M., Fenel, F., and Leisola, M. (2002) Engineering of multiple arginines into the Ser/Thr surface of *Trichoderma reesei endo*-1,4-$\beta$-xylanase II increases the thermotolerance and shifts the pH optimum towards alkaline pH, *Protein Eng. 15*, 141−145.
17. Georis, J., De Lemos Esteves, F., Lamotte-Brasseur, J., Bougnet, V., Devreese, B., Giannotta, F., Granier, B., and Frère, J.-M. (2000) An additional aromatic interaction improves the thermostability and thermophilicity of a mesophilic family 11 xylanase: Structural basis and molecular study, *Protein Sci. 9*, 466−475.
18. Arase, A., Yomo, T., Urabe, I., Hata, Y., Katsube, Y., and Okada, H. (1993) Stabilization of xylanase by random mutagenesis, *FEBS Lett. 316*, 123−127.
19. Shibuya, H., Kaneko, S., and Hayashi, K. (2000) Enhancement of the thermostability and hydrolytic activity of xylanase by random gene shuffling, *Biochem J. 349*, 651−656.
20. Sung, W. L., and Sechley, K. A. (2003) Xylanases with enhanced thermophilicity and alkalophilicity, Patent WO 03/046169.
21. Sung, W. L., Yaguchi, M., and Ishikawa, K. (1999) Modification of xylanase to improve thermophilicity, alkalophilicity and thermostability, U.S. Patent 5,866,408.
22. Morris, D., Gibbs, M., Chin, C., Koh, M.-H., Wong, K., Allison, R., Nelson, P., and Bergquist, P. (1998) Cloning of the *xynB* gene from *Dictyoglomus thermophilum* Rt46B.1 and action of the gene product on kraft pulp, *Appl. Environ. Microbiol. 64*, 1759−1765.
23. Breccia, J., Morán, A., Castro, G., and Siñeriz, F. (1998) Thermal stabilization by polyols of $\beta$-xylanase from *Bacillus amyloliquefaciens*, *J. Chem. Technol. Biotechnol. 71*, 241−245.
24. George, S., Ahmad, A., and Rao, M. (2001) A novel thermostable xylanase from *Thermomonospora* sp.: Influence of additives on thermostability, *Biores. Technol. 78*, 221−224.

25. Cobos, A., and Estrada, P. (2003) Effect of polyhydroxylic cosolvents on the thermostability and activity of xylanase from *Trichoderma reesei* QM9414, *Enzyme Microb. Technol. 33*, 810−818.
26. Törrönen, A., Harkki, A., and Rouvinen, J. (1994) Crystallographic studies on endo-1,4-$\beta$-xylanase II from *Trichoderma reesei*: two conformational states in the active site, *EMBO J. 13*, 2493−2501.
27. Törrönen, A., and Rouvinen, J. (1995) Structural comparison of two major endo-1,4-$\beta$-xylanases from *Trichoderma reesei*, *Biochemistry 34*, 847−856.
28. Fenn, J. B., Mann, M., Meng, C. K., Wong, S. F., and Whitehouse, C. M. (1989) Electrospray ionization for mass spectrometry of large biomolecules, *Science 246*, 64−71.
29. Chowdhury, K. S., Katta, V., and Chait, B. T. (1990) Probing conformational changes in proteins by mass spectrometry, *J. Am. Chem. Soc. 112*, 9013−9015.
30. Comisarow, M. B., and Marshall, A. G. (1974) Fourier transform ion cyclotron resonance spectroscopy, *Chem. Phys. Lett. 25*, 282−283.
31. Marshall, A. G., Hendrickson, C. L., and Jackson, G. S. (1998) Fourier transform ion cyclotron resonance mass spectrometry: A primer, *Mass Spectrom. Rev. 17*, 1−35.
32. Scigelova, M., Green, P. S., Giannokopulos, A. E., Rodger, A., Crout, D. H. G., and Derrick, P. J. (2001) A practical protocol for the reduction of disulfide bonds in proteins prior to analysis by mass spectrometry, *Eur. J. Mass Spectrom. 7*, 29−34.
33. Schmid, D. G., von der Mülbe, F., Fleckenstein, B., Weinschenk, T., and Jung, G. (2001) Broadband detection electrospray ionization Fourier transform ion cyclotron resonance mass spectrometry to reveal enzymatically and chemically induced deamidation reactions within peptides, *Anal. Chem. 73*, 6008−6013.
34. He, F., Hendrickson, L., and Marshall, A. G. (2000) Unequivocal determination of metal atom oxidation state in naked heme proteins: Fe(III)Myoglobin, Fe(III)Cytochrome *c*, Fe(III)Cytochrome b5, and Fe(III)Cytochrome b5 L47R, *J. Am. Soc. Mass Spectrom. 11*, 120−126.
35. Mirza, U. A., Cohen, S. L., and Chait, B. T. (1993) Heat-induced conformational changes in proteins studied by electrospray ionization mass spectrometry, *Anal. Chem. 65*, 1−6.
36. Mirza, U. A., and Chait, B. T. (1997) Do proteins denature during droplet evolution in electrospray ionization, *Int. J. Mass Spectrom. Ion Proc. 162*, 173−181.
37. Fligge, T., Przybylski, M., Quinn, J. P., and Marshall, A. G. (1998) Evaluation of heat-induced conformational changes in proteins by nanoelectrospray Fourier transform ion cyclotron resonance mass spectrometry, *Eur. J. Mass Spectrom. 4*, 401−404.
38. Katta, V., and Chait, B. T. (1993) Hydrogen/deuterium exchange electrospray ionization mass spectrometry: A new method for probing protein conformational changes in solution, *J. Am. Chem. Soc. 115*, 6317−6321.
39. Smith, D. L., Deng, Y., and Zhang, Z. (1997) Probing the noncovalent structure of proteins by amide hydrogen exchange and mass spectrometry, *J. Mass Spectrom. 32*, 135−146.
40. Wagner, D. S., and Anderreg, R. J. (1994) Conformation of cytochrome *c* studied by deuterium exchange-electrospray ionization mass spectrometry, *Anal. Chem. 66*, 706−711.
41. Zhang, Z., and Smith, D. L. (1996) Thermal-induced unfolding domains in aldolase identified by amide hydrogen exchange and mass spectrometry, *Protein Sci. 5*, 1282−1289.
42. Maier, C. S., Schimerlik, M. I., and Deinzer, M. L. (1999) Thermal denaturation of *Escherichia coli* thioredoxin studied by hydrogen/deuterium and electrospray ionization mass spectrometry: Monitoring a two-state protein unfolding transition, *Biochemistry 38*, 1136−1143.
43. Eyles, S. J., Speir, J. P., Kruppa, G. H., Gierasch, L. M., and Kaltashov, I. A. (2000) Protein conformational stability probed by Fourier transform ion cyclotron resonance mass spectrometry, *J. Am. Chem. Soc. 122*, 495−500.
44. Jänis, J., Rouvinen, J., Leisola, M., Turunen, O., and Vainiotalo, P. (2001) Thermostability of endo-1,4-$\beta$-xylanase II from *Trichoderma reesei* studied by electrospray ionization Fourier transform ion cyclotron resonance MS, hydrogen/deuterium-exchange reactions and dynamic light scattering, *Biochem. J. 356*, 453−460.
45. Glasoe, P. K., and Long, F. A. (1960) Use of glass electrodes to measure acidities in deuterium oxide, *J. Phys. Chem. 64*, 188−190.
46. Caravatti, P., and Alleman, M. (1991) The "Infinity" cell: A new trapped-ion cell with radiofrequency covered trapping electrodes for Fourier transform ion cyclotron resonance mass spectrometry, *Org. Mass Spectrom. 26*, 514−518.
47. Palmblad, M., Håkansson, K., Håkansson, P., Feng, X., Cooper, H. J., Giannakopulos, A. E., Green, P. S., and Derrick, P. J. (2000) A 9.4 T Fourier transform ion cyclotron resonance mass spectrometer: Description and performance, *Eur. J. Mass Spectrom. 6*, 267−275.
48. Barrow, M. P., McDonnell, L. A., Feng, X., Walker, J., and Derrick, P. J. (2003) Determination of the nature of naphthenic acids present in crude oils using nanospray Fourier transform ion cyclotron resonance mass spectrometry: The continued battle against corrosion, *Anal. Chem. 75*, 860−866.
49. Tenkanen, M., Puls, J., and Poutanen, K. (1992) Two major xylanases of *Trichoderma reesei*, *Enzyme Microb. Technol. 14*, 566−574.
50. Saarelainen, R., Paloheimo, M., Fagerström, R., Suominen, P. L., and Nevalainen, K. M. H. (1993) Cloning, sequencing and enhanced expression of the *Trichoderma reesei* endoxylanase II (pI 9) gene xln2, *Mol. Gen. Genet. 241*, 497−503.
51. Gavel, Y., and von Heijne, G. (1990) Sequence differences between glycosylated and non-glycosylated N-X-T/S acceptor sites: implications for protein engineering, *Protein Eng. 3*, 433−442.
52. Shakin-Eshleman, S. H., Kasturi, L., Spitalnik, S. L., and Mellquist, J. L. (1998) The amino acid following an Asn-X-Ser/Thr sequon is an important determinant of N-linked core glycosylation efficiency, *Biochemistry 37*, 6833−6837.
53. Klarskov, K., Piens, K., Ståhlberg, J., Høj, P. B., Van Beeumen, J., and Claeyssens, M. (1997) Cellobiohydrolase I from *Trichoderma reesei*: Identification of an active-site nucleophile and additional information on sequence including the glycosylation pattern of the core protein, *Carbohydr. Res. 304*, 143−154.
54. Harrison, M. J., Nouwens, A. S., Jardine, D. R., Zachara, N. E., Gooley, A. A., Nevalainen, H., and Packer, N. H. (1998) Modified glycosylation of cellobiohydrolase I from a high cellulase-producing mutant strain of *Trichoderma reesei*, *Eur. J. Biochem. 256*, 119−127.
55. Guy, P., Rémigy, H., Jaquinod, M., Bersch, B., Blanchard, L., Dolla, A., and Forest, E. (1996) Study of the new stability properties induced by amino acid replacement of tyrosine 64 in cytochrome *c*533 from *Desulfovibrio vulgaris* Hildenborough using electrospray ionization mass spectrometry, *Biophys. Biochem. Res. Commun. 218*, 97−103.
56. Ghaemmaghami, S., Fitzgerald, M. C., and Oas, T. G. (2000) A quantitative, high-throughput screen for protein stability, *Proc. Natl. Acad. Sci. U.S.A. 97*, 8296−8301.
57. Powell, K. D., and Fitzgerald, M. C. (2001) Measurements of protein stability by H/D exchange and matrix-assisted laser desorption/ionization mass spectrometry using picomoles of material, *Anal. Chem. 73*, 3300−3304.
58. Vriend, G., Berendsen, H. J. C., van der Burg, B., Venema, G., and Eijsink, V. G. H. (1998) Early steps in the unfolding of thermolysin-like proteases, *J. Biol. Chem. 273*, 35074−35077.

BI049597B